

Radiation effects of electrons on multilayer $FePS_2$ studied withlaser plasma accelerator

Meng Peng(彭猛), Jun-Bo Yang(杨俊波), Hao Chen(陈浩), Bo-Yuan Li(李博源), Xu-Lei Ge(葛绪雷), Xiao-Hu Yang(杨晓虎), Guo-Bo Zhang(张国博), and Yan-Yun Ma(马燕云)

Citation: Chin. Phys. B, 2022, 31 (**8**): 086102. DOI: 10.1088/1674-1056/ac5c34
Journal homepage: http://cpb.iphy.ac.cn; http://iopscience.iop.org/cpb

What follows is a list of articles you may be interested in

Structural evolution and bandgap modulation of layered *β*-$GeSe_2$ single crystal under high pressure

Hengli Xie(谢恒立), Jiaxiang Wang(王家祥), Lingrui Wang(王玲瑞), Yong Yan(闫勇), Juan Guo(郭娟), Qilong Gao(高其龙), Mingju Chao(晁明举), Erjun Liang(梁二军), and Xiao Ren(任霄)

Chin. Phys. B, 2022, 31 (**7**): 076101. DOI: 10.1088/1674-1056/ac6db8

Raman spectroscopy investigation on the pressure-induced structural and magnetic phase transition in two-dimensional antiferromagnet $FePS_3$

Hong Zeng(曾鸿), Tingting Ye(叶婷婷), Peng Cheng(程鹏), Deyuan Yao(姚德元), and Junfeng Ding(丁俊峰)

Chin. Phys. B, 2022, 31 (**5**): 056109. DOI: 10.1088/1674-1056/ac5a41

Transition state and formation process of Stone—Wales defects in graphene

Jian-Hui Bai(白建会), Yin Yao(姚茵), and Ying-Zhao Jiang(姜英昭)

Chin. Phys. B, 2022, 31 (**3**): 036102. DOI: 10.1088/1674-1056/ac20c5

Sphere-shaped SiGe micro/nanostructures with tunable Ge composition and size formed by laser irradiation

Xinxin Li(李欣欣), Zhen Deng(邓震), Sen Wang(王森), Jinbiao Liu(刘金彪), Jun Li(李俊), Yang Jiang(江洋), Ziguang Ma(马紫光), Chunhua Du(杜春花), Haiqiang Jia(贾海强), Wenxin Wang(王文新), and Hong Chen(陈弘)

Chin. Phys. B, 2021, 30 (**9**): 096104. DOI: 10.1088/1674-1056/ac0347

Geant4 simulation of proton-induced single event upset in three-dimensional die-stacked SRAM device

Bing Ye(叶兵), Li-Hua Mo(莫莉华), Tao Liu(刘涛), Jie Luo(罗捷), Dong-Qing Li(李东青), Pei-Xiong Zhao(赵培雄), Chang Cai(蔡畅), Ze He(贺泽), You-Mei Sun(孙友梅), Ming-Dong Hou(侯明东), Jie Liu(刘杰)

Chin. Phys. B, 2020, 29 (**2**): 026101. DOI: 10.1088/1674-1056/ab5fc4

Radiation effects of electrons on multilayer $FePS_3$ studied with laser plasma accelerator

Meng Peng(彭猛)[1], Jun-Bo Yang(杨俊波)[1,†], Hao Chen(陈浩)[2], Bo-Yuan Li(李博源)[3], Xu-Lei Ge(葛绪雷)[3], Xiao-Hu Yang(杨晓虎)[1], Guo-Bo Zhang(张国博)[1], and Yan-Yun Ma(马燕云)[4,‡]

[1] *Department of Physics, National University of Defense Technology, Changsha* 410072, *China*
[2] *College of Physics and Optoelectronic Engineering, Shenzhen University, Shenzhen* 518000, *China*
[3] *Key Laboratory for Laser Plasmas (MoE), School of Physics and Astronomy, Shanghai Jiao Tong University, Shanghai* 200240, *China*
[4] *College of Advanced Interdisciplinary Studies, National University of Defense Technology, Changsha* 410073, *China*

(Received 4 November 2021; revised manuscript received 12 February 2022; accepted manuscript online 10 March 2022)

Space radiation with inherently broadband spectral flux poses a huge danger to astronauts and electronics on aircraft, but it is hard to simulate such feature with conventional radiation sources. Using a tabletop laser-plasma accelerator, we can reproduce exponential energy particle beams as similar as possible to these in space radiation. We used such an electron beam to study the electron radiation effects on the surface structure and performance of two-dimensional material ($FePS_3$). Energetic electron beam led to bulk sample cleavage and damage between areas of uneven thickness. For the $FePS_3$ sheet sample, electron radiation transformed it from crystalline state to amorphous state, causing the sample surface to rough. The full widths at the half maximum of characteristic Raman peaks became larger, and the intensities of characteristic Raman peaks became weak or even disappeared dramatically under electron radiation. This trend became more obvious for thinner samples, and this phenomenon was attributed to the cleavage of P–P and P–S bonds, destabilizing the bipyramid structure of $[P_2S_6]^{4-}$ unit. The results are of great significance for testing the maximum allowable radiation dose for the two-dimensional material, implying that $FePS_3$ cannot withstand such energetic electron radiation without an essential shield.

Keywords: space radiation, laser–plasma interaction, two-dimensional material, Raman spectroscopy

PACS: 61.48.De, 68.65.–k, 72.90.+y **DOI:** 10.1088/1674-1056/ac5c34

1. Introduction

Space radiation is one of the substantial threats to spacecraft and satellites because it can severely damage solar cells and electronics onboard.[1] With the continuous deepening of human space exploration, the demands on spacecraft performance are increasing. All space agencies around the world are constantly developing various countermeasures to deal with this threat. Space radiation, which has a plenitude of different types and origins, can be extremely versatile. Space radiation is usually composed of various particles, such as electrons, protons, ions, and photons. Moreover, the energy spectra of radiation belt are very broadband, spanning multiple orders of magnitude.[1,2] Space radiation belts exist in the five strongly magnetized planets in solar system, namely, Earth, Jupiter, Saturn, Uranus, and Neptune.[3–5] According to the model based on the measurements of Pioneer and Voyager detections, the electron energy in Jupiter's radiation belt can reach 100 MeV, which is much higher than that in Earth's radiation belt.[5–8]

In planetary radiation belts, energetic electrons are accelerated to form directional spectra fluxes characterized by a power-law or exponential decline towards higher energies. In contrast to space radiation, laboratory's space radiation test facilities characterized by linacs or cyclotrons cannot produce broadband spectra, but instead monoenergetic beams, resulting in completely different energy deposition on the device.[9] Based on the chirped pulse amplification (CPA),[10] today's laser system can generate power up to petawatt-regime to produce relativistic electron beam by laser–plasma interaction.[11,12] Electron beams with low energy divergence and exponential energy distribution emitted from laser-plasma accelerator (LPA) are similar to the conditions in space radiation, contributing to a booming research field, especially in the field of space radiation.[2,8,12] LPA is a workable advanced tool as a complementary source for space radiation testing. In 2017, Hidding *et al.*[2] used LPA to reproduce the broadband Van-Allen belt level electron beam for systematically exploring the degradation of optocouplers, and a significant electronics degradation characterized straightforwardly by the current transfer ratio was acquired with such laboratory-made space radiation.

The harsh radiation environment has a severe impact on the reliability of conventional silicon-based devices. The undesirable phenomena such as single event effect, total dose effect, and displacement damage, can adversely affect their performance.[13–16] Now, quantum tunneling is setting a hard

†Corresponding author. E-mail: yangjunbo@nudt.edu.cn
‡Corresponding author. E-mail: yanyunma@126.com

© 2022 Chinese Physical Society and IOP Publishing Ltd

limit for further miniaturization of silicon-based electronics at nanoscale technology nodes, but the adoption of novel material and/or device structure is considered beyond this limit. Of particular interest is the two-dimensional (2D) material such as graphene,[17–20] transition metal dichalcogenide (TMD),[21–23] and black phosphorus (BP).[24–26] Their intrinsically large specific area, low power requirement, and chemical stability make devices based on 2D material a promising candidate for space instrumentation.[14] The 2D material-based integrated electronics have a smaller sensitive volume, demonstrating stronger protection against single event effects.[27] However, zero bandgap limits the application of graphene in the field of optoelectronics.[17,18] BP (0.3 eV) and TMD (< 2.0 eV) have a small bandgap that hinders the potential optoelectronic application at higher energy. Recently, 2D layered metal phosphorus trichalcogenides ($M\mathrm{PS_3}$, $M =$ Fe, Ni, Mn, Zn, etc.)[28–31] have received enormous attention for the excellent electronic, optical and magnetic properties derived from their electronic structure and energy band. In this article, we study the exponential energy electron beam produced by LPA for the 2D material ($\mathrm{FePS_3}$) testing, which has potential space application. A series of characterizations have been performed on the $\mathrm{FePS_3}$ sample before and after electron radiation for radiation damage analysis, and the detailed discussion and conclusion are given in Section 3.

2. Experimental details

2.1. Preparation and characterization of $\mathrm{FePS_3}$

The crystal structure of $\mathrm{MPS_3}$ has been extensively studied in the latter half of the 20$^{\mathrm{th}}$ century. The $\mathrm{MPS_3}$ family forms a stacked structure, while the interlayer is connected through weak Van Der Waals force. Each $[\mathrm{P_2S_6}]^{4-}$ unit is located at the center of the regular hexagon with 6 corners occupied by transition metal ion (M^{2+}). The M^{2+} ion sits at 4m position, forming a honeycomb structure surrounded by 6 sulfur ions with trigonal symmetry. These sulfur ions themselves are connected to two P–P ion pairs above and below the metal plane like a dumbbell (see Fig. 1(a)), forming a monoclinic symmetrical $C2/m$ structure.[31–36] The attractive feature of $M\mathrm{PS_3}$ compound is that their optical properties are determined by the M-site element, and the range of absorption photon energy is between 1.5–3.5 eV. In addition, their ability to accommodate the extrinsic species in Van Der Waals gap can significantly modify the magnetic, optical and electrical properties.[34,37] In $\mathrm{FePS_3}$, each $\mathrm{Fe^{2+}}$ ion is ferromagnetically coupled with two of the three nearest neighbors, and antiferromagnetically with the third one in a layer, meaning that the $\mathrm{Fe^{2+}}$ ion participates in competitive ferromagnetic and antiferromagnetic couplings. The $\mathrm{FePS_3}$ magnetic cell is doubled along the c-axis with respect to the crystallographic one, affecting $[\mathrm{P_2S_6}]^{2-}$ vibration, i.e., the $\mathrm{A_{1g}^{(1)}}$ is strongly activated. The radiation effect on $M\mathrm{PS_3}$ is of particular interest, while radiation effects on the electrical properties and optical characteristics of graphene and TMD have been studied extensively, less study investigates these effects on $\mathrm{MPS_3}$ and other 2D materials. In 2019, Junbo Yang *et al.*[33] investigated the modification of $\mathrm{FePS_3}$ structure via $\mathrm{Ga^+}$ ion radiation. The damage of bipyramid structure of $[\mathrm{P_2S_6}]^{4-}$ unit and break of the P–P band and the P–S band led the $\mathrm{FePS_3}$ sample to gradually thinner, and the characteristic peaks had an obvious change after $\mathrm{Ga^+}$ ion radiation. While testing directly in space environment for 2D material-based device is possible, a more practical way is to use radiation sources on Earth instead of space environment. Herein, we exfoliated the bulk $\mathrm{FePS_3}$ and then transferred it onto Silicon substrate capped by 285 nm $\mathrm{SiO_2}$. A broadband electron flux generated from LPA has been used to study the radiation damage on $\mathrm{FePS_3}$ samples.

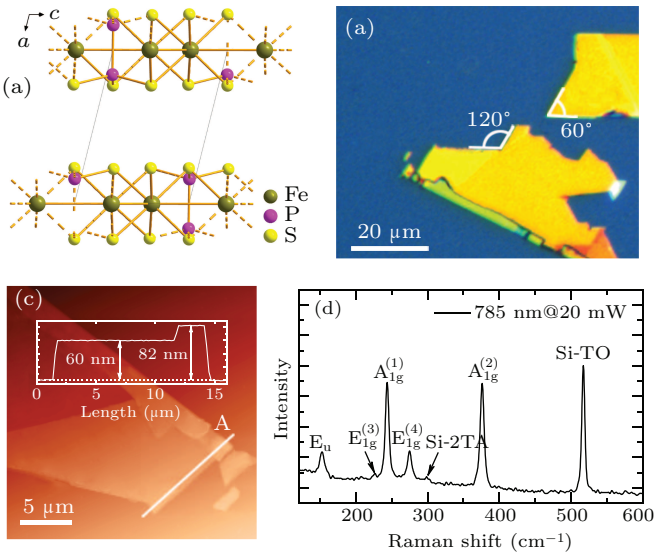


Fig. 1. (a) Schematic crystal structure of $\mathrm{FePS_3}$. (b) Brightfield microscope image of cleaved sheet samples exfoliated onto an oxidized silicon substrate. (c) AFM topography image of $\mathrm{FePS_3}$ sample, and the height profiles along line A. (d) The typical Raman spectrum of $\mathrm{FePS_3}$ sample showing $\mathrm{E_u}$, $\mathrm{E_{1g}^{(3)}}$, $\mathrm{A_{1g}^{(1)}}$, $\mathrm{E_{1g}^{(4)}}$, $\mathrm{A_{1g}^{(2)}}$, Si-2TA, and Si-TO peaks.

An optical microscope (BX41M-LED, Olympus) has been used to characterize the $\mathrm{FePS_3}$ samples. In the case of exfoliated $\mathrm{FePS_3}$ samples, the region edges and boundaries between different layers often run in parallel or are arranged at angles close to 60° and 120°[34] (see Fig. 1(b)). This observation is due to the crack-propagation along the crystal axis of high-symmetry during exfoliation. The $\mathrm{FePS_3}$ samples comprising areas of tens of layers with 2–20 μm lateral dimensions have been scanned by the atomic force microscopy (AFM, NT-MDT Solver SPM &SNOM). Figure 1(c) presents the AFM topography image along height profiles. Raman spectroscopy (Senterra, Bruker), as a non-destructive characterization technique, has been used to test the property of $\mathrm{FePS_3}$ at room temperature. According to

previous reports,[34,38] the Raman modes originate from the $[P_2S_6]^{4-}$ unit vibration and the iron atom vibration (88 cm^{-1} and 95 cm^{-1}).[38] As far as the $[P_2S_6]^{4-}$ vibration is concerned, it has ten Raman active modes, including five in-plane E_g modes ($E_g^{(1)}$ (128 cm^{-1}), $E_g^{(2)}$ (173.7 cm^{-1}), $E_g^{(3)}$ (231.1 cm^{-1}), $E_g^{(4)}$ (278.8 cm^{-1}), $E_g^{(5)}$ (557.3 cm^{-1})), three out-of-plane A_g modes ($A_{1g}^{(1)}$ (252.3 cm^{-1}), $A_{1g}^{(2)}$ (381 cm^{-1}), $A_{1g}^{(3)}$ (586.5 cm^{-1})), and two second-order A_g modes ($2A_{1g}^{(2)}$ (809.7 cm^{-1}), $2A_{1g}^{(3)}$ (1181.5 cm^{-1})).[38] As for multilayer $FePS_3$ sample, the $[P_2S_6]^{4-}$ unit is doubled along the *c*-axis, and the out-of-plane vibration in contiguous layers is activated, resulting in E_u (155 cm^{-1}) mode appearance.[38] The Raman spectrum of sheet sample excited by 785 nm laser on SiO_2 substrate is shown in Fig. 1(d). By considering the lower energy of 785 nm laser, only the E_u, $E_{1g}^{(1)}$, $A_{1g}^{(1)}$, $E_{1g}^{(1)}$, and $A_{1g}^{(2)}$ peaks were measured. It has no $A_{1g}^{(3)}$ mode stiffening in Raman spectrum because the vertical components of sulfur atom plane vibrations are so weak that they can be affected by the magnetic ordering.[32,39]

2.2. Electron radiation

In 1979, laser electron acceleration was proposed by Tajima and Dawson.[40] In their theory, when an intense focused laser pulse ($I \geq 10^{18}$ W/cm^2) propagates through the underdense plasma, this plasma will excite a relativistic plasma wave with a field amplitude of 100 GV/m. This plasma wave passes through the plasma at the same speed of laser.[12,41] Massive charge displacements cause a high electric wake-field for electron acceleration to relativistic energy in a very short distance. The radiation damage experiment has been performed with a compact state-of-the-art Ti:sapphire laser system at Shanghai Jiao Tong University.[42] Here, the laser pulse with an energy of $E \sim 5.8$ J was delivered in 29 fs over a 30 μm diameter focus. The laser was focused on a gas-jet target by off-axis parabola (OAP) where the gas-jet ejected the mixed gas (0.5% N_2 + 99.5% He) at each shot to produce a broadband electron beam by self-truncated ionization injection.[42] The whole experimental process was carried out in a vacuum chamber, as described in Fig. 2.

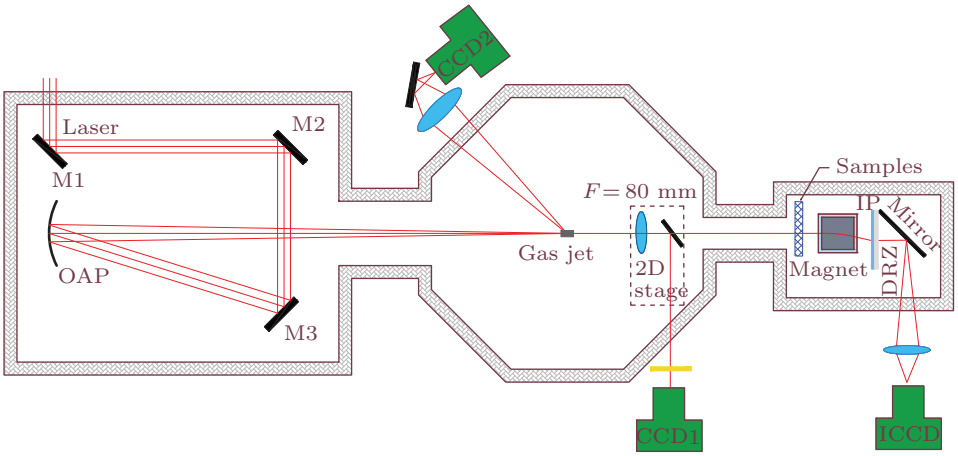


Fig. 2. The setup of the radiation chamber for online monitoring electron beam. The indent laser system was strongly focused on the gas jet by OAP where the radiation was produced. Focus diagnostic microscope objective (2D stage), permanent magnet-based spectrometer, IP, and DRZ in the forward direction were positioned next to the gas jet.

An infrared camera (CCD1, Spiricon OPHIR Photonics) and 2D stage were used to monitor dynamically the focused laser spot when adjusting the laser path to maximize the laser intensity on the gas jet. The top-view image of plasma channel formed by laser–plasma interaction was captured by a 12-bit CCD camera (CCD2, Pixelfly). The electron beam was recorded by the magnetic spectrometer which consists of a permanent dipole magnet, an Image Stack (IP, Fusji), a scintillator screen (DRZ, Mitsubishi Chemical), and an intensified charge-coupled device (ICCD, Andor) camera. The dipole magnet was 16 cm long, 1.0 T magnetic field strength with a 1 cm gap. The direction of magnetic field in the gap was perpendicular to its horizontal plane during installation. The distance between the exit of dipole magnet and the IP was 16.5 cm, which fully resolves the peak electron energy up to $\sim$ 400 MeV. The energetic electron flux could penetrate the IP to image on the DRZ, and then the fluorescence signals emitted from DRZ were recorded by ICCD online. A cumulative electron signals with 5 shots in IP are presented in Fig. 3(a). Based on the gyroradius of the electron trajectory in dipole magnet and electron signals recorded by IP, an average electron number of 1.2×10^7 per shot is produced. The fluence of LPA-produced electron beam per shot is approximately equivalent to the electron beams with energies greater than 0.2 MeV in Earth's radiation belt. The broadband electron spectrum is depicted in Fig. 3(b) (black line).

In order to make $FePS_3$ samples with cross-section of about 1×1 cm fully irradiated by an electron beam with a few milliradian divergence, an 8 mm thick aluminum foil has been used to enlarge the electron beam spot. Meanwhile, an InSe film has been used to monitor the uniformity and spot size of the electron beam, while the magnetic spectrometer and DRZ

were positioned in the front of $FePS_3$ sample for dynamic monitoring electron beam. The schematic diagram of radiation test is depicted in Fig. 4(a), where the accumulated electron beams with 3 shots were irradiated on the $FePS_3$ samples. The transportation process of energetic electron beam in aluminum foil has been simulated with Geant4 (Version 4.10.7).[43,44] The "FTFP_BERTGE" physics package was used to describe the transportation of energetic electrons and secondary particles. It was assumed that a plane particle source of 1 mm radius, 50 milliradian divergence degree shot electrons to aluminum foil after 50 cm flight in vacuum. Based on the simulation results, the spot radius of the outgoing electron beam was expanded to 5 mm, fully covering the surface of testing samples (see Fig. 4(b)). The simulated outgoing electron spectrum is presented in Fig. 3(b) (red line).

The energetic electron beams produced by LPA are well beyond the energy limit of Earth's radiation belt where the majority of electrons have energies up to 15 MeV. However, it shall be pointed out that the most important aspect is the exponential electron spectrum produced by LPA.[12] Moreover, based on the simulation results, the deposited energies to $FePS_3$ sample via electron–nucleus scattering are rather constant for electron energy range above 3 MeV (see Fig. 5). The total absorbed dose of $FePS_3$ sample irradiated by LPA-produced electron beams is about 1.2 mGy, which is 10% higher than that produced by electron beams at geosynchronous orbit at the same electron intensity.

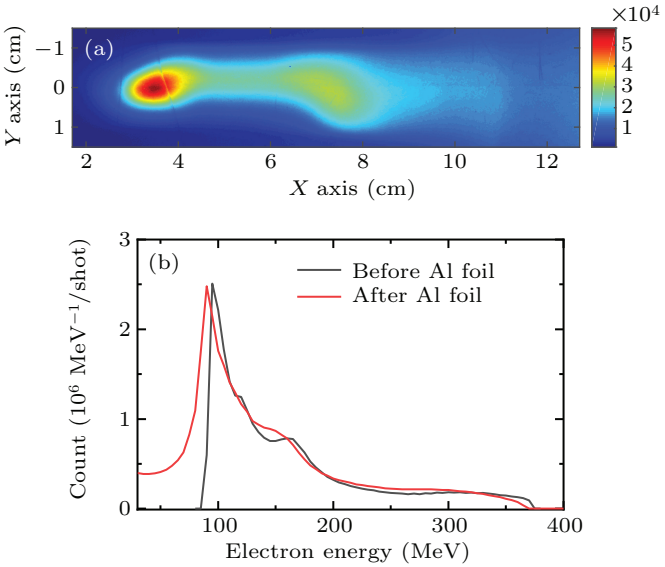


Fig. 3. The exponential electron beam produced from LPA. (a) The raw information of electron beams obtained by IP. (b) The induced broadband electron spectra before (black line, the experimental result) and after (red line, the simulated result) passing through Al foil.

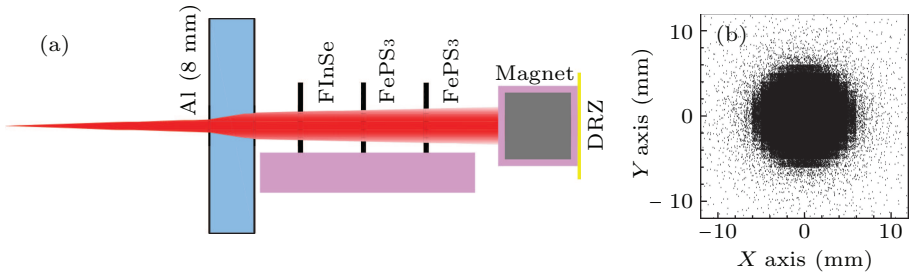


Fig. 4. (a) Schematic diagram of the electron beam for radiation test. (b) The spot size of electron flux after propagating Al foil.

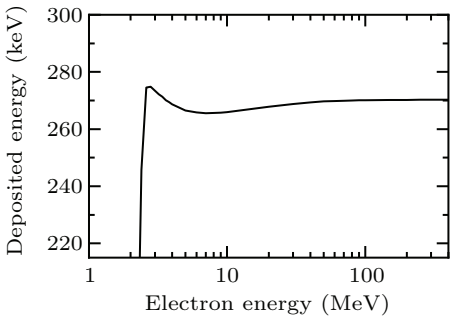


Fig. 5. The simulated results of deposited energy for electron energy from 3 MeV to 400 MeV in the $FePS_3$ sheet sample.

3. Results and discussion

Electron stopping is mainly controlled by inelastic scattering between the incoming energetic electron beam and the electrons in the target.[45] Inelastic scattering can excite target electrons to relatively high energy (keV), which can transfer electron excitation energy away from the central region of the lattice, causing damage far away from the collision region. When the transferred energy is large enough to exceed the threshold for target atom displacing from lattice position, it causes to ionization and bond breakage. Once electron beams transfer enough energy, or numerous inelastic scatterings occur close to each other, the cascade process develops into a complex multi-body phenomenon, leading to the lattice breakup. The region of overlapping collisions can be regarded as "hot", called a "heat spike",[46–48] which may lead to intense heating of crystal lattice and damage to the cylindrical heat spikes.[49] Near the sample surface, the heat spike can lead to massive sputtering evaporation.[50] The optical image of InSe film exposed to the energetic electron beam is presented in Fig. 6(a). There are significantly light spots corresponding to the thinner area formed from the massive evaporation, whereas the optical characteristics of InSe film also indicate that the electron flux uniformity was good after propagating Al foil. The energies transferred to the $FePS_3$ sample were

much larger than the bond energy and Van Der Waals gap, causing the bond to broke and massive particle evaporation. As a result, electron radiation led to bulk sample cleavage and damage between areas of uneven thickness (see Figs. 6(b)–6(c)).

The energy of electron beam far exceeds the threshold for knock-on damage, and hole formation to the crystal lattice can be initiated at energy as low as tens of keV.[51] The optical image of sheet sample after electron radiation is presented in Fig. 7(a). It has numerous cyan holes on the $FePS_3$ surface caused by electron sputtering. The electron radiation effect on the surface topography of $FePS_3$ was also characterized with AFM at ambient temperature, while the surface image and the height information of multilayer $FePS_3$ sample following radiation are shown in Figs. 7(b)–7(c). The thin sheet sample has smaller average roughness (R_a) than the thick sample, which is ascribed to more average energy acquired by sample target atoms during radiation and impurities on the surface. During the preparation of sheet samples, H_2O and O_2 molecules adhere inevitably to the sample surface. Electron radiation breaks the structure of $[P_2S_6]^{4-}$, and the dangling bonds of S and P can combine H_2O and O_2 molecules to form S=O and P=O bonds.

The normalized Raman spectra of the as-prepared and electron-irradiated $FePS_3$ samples are shown in Figs. 8(a)–8(c). We find that the full width at half maximums of E_u peak, $A_{1g}^{(1)}$ peak, $E_{1g}^{(4)}$ peak, and $A_{1g}^{(2)}$ peak have a significant increase, which is due to the formation of electron-induced defects in $FePS_3$ sheet sample. The normalized intensities of all Raman characteristic peaks decrease sharply or even disappear, and the central frequencies of the Raman peaks undergo a significant blue-shift, indicating that electron radiation can affect the surface structure of $FePS_3$ sample. Based on the "three-stage model" proposed by Ferrari and Robertson,[52] the observed change indicates that the transformation of the $FePS_3$ sample, from crystalline $FePS_3$ to amorphous $FePS_3$, was occurring. The cleavage of P–P and P–S bonds by electron radiation destabilizes the bipyramid structure of $[P_2S_6]^{4-}$ unit, leading to the vibration mode of in-plane suppressed. The intensities of $E_{1g}^{(4)}$ peak corresponding to tangential vibration of the P–P band and in-plane vibration of $[P_2S_6]^{4-}$ unit,[33] $A_{1g}^{(1)}$ peak and $A_{1g}^{(2)}$ peak corresponding to stretching vibration of the P–P band and out-of-plane vibration of $[P_2S_6]^{4-}$ unit weakened to some extent, while the Eu peak corresponding to the out-of-plane vibration of two $[P_2S_6]^{4-}$ units in adjacent layers tended to disappear in the Raman spectrum under electron radiation.[33] Moreover, electron radiation broke Fe^{2+} ion competition in ferromagnetic and antiferromagnetic coupling, leading to the very small shifts of all Raman peaks, while all Raman vibrations are very sensitive to the interlayer magnetic coupling in the magnetic superstructure.

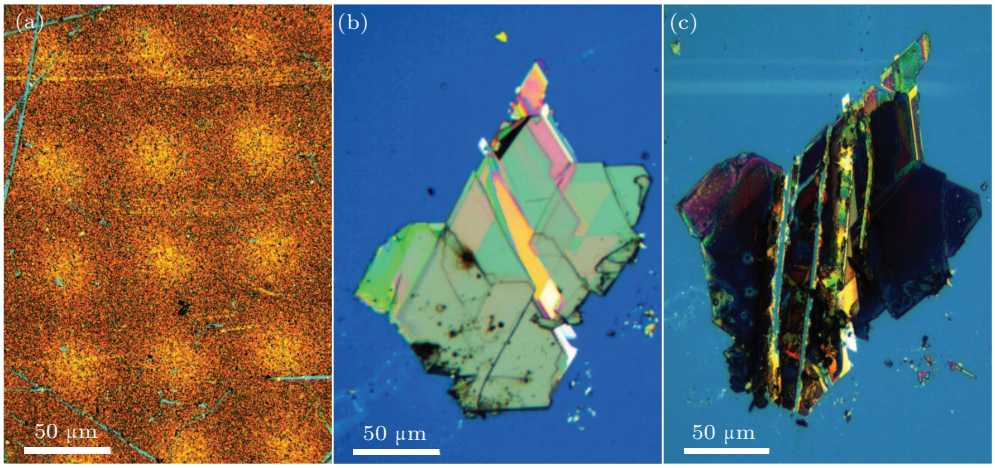


Fig. 6. (a) Optical image of InSe with obvious light spots after radiation. (b) Optical image of bulk $FePS_3$ sample before radiation. (c) The electron-induced cleavage of bulk $FePS_3$ sample after radiation.

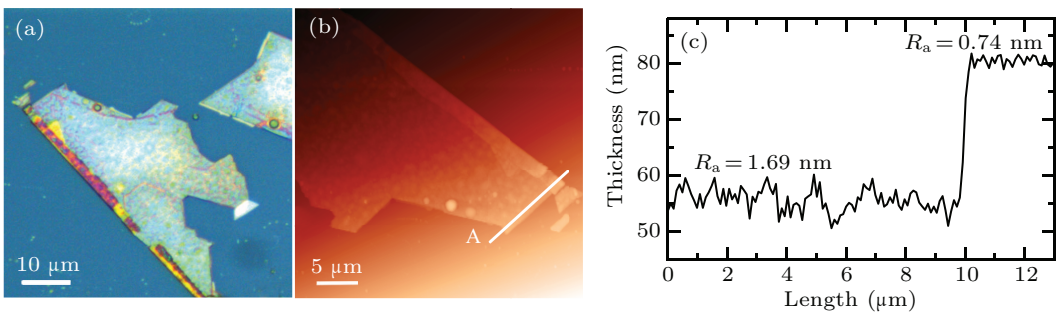


Fig. 7. (a) Brightfield microscope image of sheet samples after electron radiation. (b) AFM surface topography of $FePS_3$ sheets following energetic electron radiation. (c) The cross-sectional height along line A in (b).

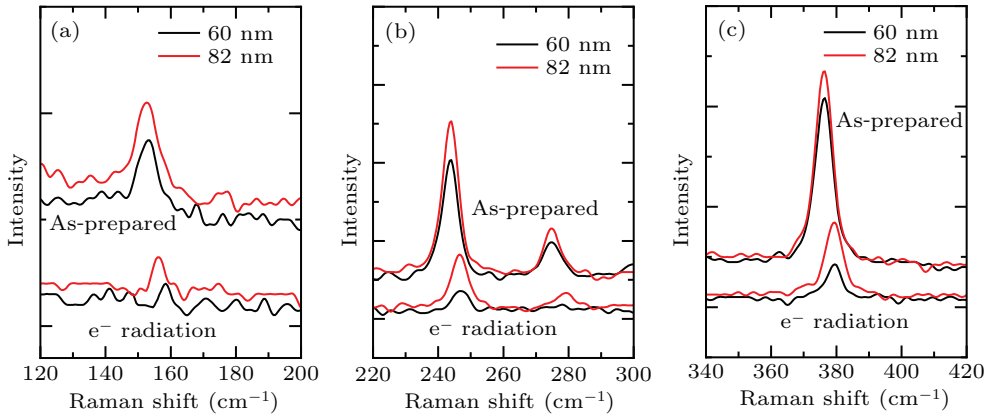


Fig. 8. The Raman spectra of $FePS_3$ sample before and after electron radiation. (a) Out-of-plane vibration: E_u mode. (b) Out-of-plane vibration: $A_{1g}^{(1)}$ mode and in-plane vibration: $E_{1g}^{(4)}$ mode. (c) Out-of-plane vibration: $A_{1g}^{(2)}$ mode.

4. Conclusion

In combination with the established conventional radiation source, LPA, as a complementary radiation source, can allow us to reproduce space radiation for electronic tests. In this work, a compact state-of-the-art Ti:sapphire laser system at a laser intensity of $I = 2.8 \times 10^{19}$ W/cm^2 has been used to produce broadband electron beams for studying space radiation effects on the 2D material. In this experiment of laser-plasma interaction, we have produced an exponential energetic electron beam with an average intensity of 1.4×10^7/shot.

The effects of electron beam radiation on tens of layers $FePS_3$ samples have been systematically investigated with different kinds of characterization tools. Electron radiation led to the bulk sample cleavage and damage between areas of uneven thickness, while the energetic electron beam caused massive sputtering and ablation of the $FePS_3$ sheet sample, resulting in the surface of $FePS_3$ samples rough dramatically. Electron radiation also caused severe damage on the bipyramid structure of $[P_2S_6]^{4-}$ unit and the cleavage of P–P and P–S bonds, resulting in all the characteristic peaks sharply weakened to some extent, or even disappearing. It has a radiation threshold on the 2D material and device for normal operation under such harsh electron radiation. Our results pave the way towards testing the property of 2D materials under intense radiation and the allowable radiation dose for the application of 2D material and device.

Acknowledgements

Project supported by the National Natural Science Foundation of China (Grant No. 11975308), the Strategic Priority Research Program of Chinese Academy of Sciences (Grant No. XDA25050200), and Science Challenge Project (Grant No. TZ2018001).

References

[1] Novikov L S, Mileev V N, Voronina E N, Galanina L I and Sinolits V V 2009 *J. Surf. Invest.: X-ray, Synchrotron & Neutron Techn.* **3** 199
[2] Hidding B, Karger O, Königstein T, *et al*. 2017 *Sci. Rep.* **7** 42354
[3] Mauk B H and Fox N J 2010 *J. Geophys. Res.* **115** A12220
[4] Horne R B, Thorne R M, Shprits Y Y, *et al*. 2005 *Nature* **437** 227
[5] Thorne R, Glauert S, Menietti J, *et al*. 2008 *Nat. Phys.* **4** 301
[6] Bolton S J, Janssen M, Thorne R, *et al*. 2002 *Nature* **415** 987
[7] Tao X, Thorne R M, Horne R B, Ni B, Menietti J D, Shprits Y Y and Gurnett D A 2011 *J. Geophys. Res.* **116** A01206
[8] Königstein T, Karger O, Pretzler G, Rosenzweig J B and Hidding B 2012 *J. Plasma Phys.* **78** 383
[9] KÖnigstein T, Karger O, Pretzler G, *et al*. 2012 *J. Plasma Phys.* **78** 383)
[10] Strickland D and Mourou G 1985 *Opt. Commun.* **56** 219
[11] Malka V, Fritzler S, Lefebvre E, *et al*. 2002 *Science* **298** 1596
[12] Hidding B, Konigstein T, Willi O, *et al*. 2011 *Nucl. Instrum. Meth. A* **636** 31
[13] Alexandrou K, Masurkar A, Edrees H, Wishart J F, Hao Y F, Nicholas P, Hone J and Kymissis I 2016 *Appl. Phys. Lett.* **109** 153108
[14] Vogl T, Sripathy K, Sharma A, *et al*. 2019 *Nat. Commun.* **10** 1202
[15] Li G C and Li S T 2019 *Acta Phys. Sin.* **68** 239401 (in Chinese)
[16] Liu J and Zhang H B 2019 *Acta Phys. Sin.* **68** 059401 (in Chinese)
[17] Novoselov K S, Geim A K, Morozov S V, *et al*. 2004 *Science.* **306** 666
[18] Geim A K and Novoselov K S 2007 *Nat. Mater.* **6** 183
[19] Han M X, Ji Z Y, Shang L W, *et al*. 2011 *Chin. Phys. B* **20** 86102
[20] Koziol Z, Gawlik G and Jagielski J. 2019 *Chin. Phys. B* **28** 096101
[21] Huang X, Zeng Z and Zhang H 2013 *Chem. Soc. Rev.* **42** 1934
[22] Novoselov K S, Jiang D, Schedin F, *et al*. 2005 *Proc. Natl. Acad. Sci. USA* **102** 10451
[23] Chhowalla M, Shin H S, Eda G, *et al*. 2013 *Nat. Chem.* **5** 263
[24] Kou L, Chen C and Smith S C 2015 *J. Phys. Chem. Lett.* **6** 2794
[25] Abbas A N, Liu B, Chen L, *et al*. 2015 *ACS Nano* **9** 5618
[26] Lu J, Jing W, Carvalho A, *et al*. 2015 *ACS Nano* **9** 10411
[27] Koester S J 2012 *IEEE Nuclear and Space Radiation Effects Conference*, July 16–20, 2012, Miami, America, p. 5
[28] Joy P A and Vasudevan S 1992 *Phys. Rev. B.* **46** 5425
[29] Le Flem G, Brec R, Ouvard G, *et al*. 1982 *J. Phys. Chem. Solids.* **43** 455
[30] Rule K C, McIntyre G J, Kennedy S J, *et al*. 2007 *Phys. Rev. B.* **76** 134402
[31] Du K Z, Wang X Z, Liu Y, *et al*. 2016 *ACS Nano* **10** 1738
[32] Cheng Z, Shifa T A, Wang F, *et al*. 2018 *Adv. Mater.* **30** 1707433
[33] Xu H, Wang S, Ouyang J, *et al*. 2019 *Sci. Rep.* **9** 15219
[34] Kuo C T, Neumann M, Balamurugan K, *et al*. 2016 *Sci. Rep.* **6** 20904
[35] Susner M A, Chyasnavichyus M, McGuire M A, *et al*. 2017 *Adv. Mater.* **29** 1602852
[36] Long G, Zhang T, Cai X, *et al*. 2017 *ACS Nano* **11** 11330
[37] Brec R, Schleich D M, Ouvrard G, *et al*. 1979 *Inorg. Chem.* **18** 1814
[38] Wang X Z, Du K Z, Liu Y Y F, Hu P, Zhang J, Zhang Q, Owen M H S, Lu X, Gan C K, Sengupta P, Kloc C and Xiong Q H 2016 *2D Mater.* **3** 031009
[39] Jenjeti R N, Kumar R, Austeria M P, *et al*. 2018 *Sci. Rep.* **8** 8586
[40] Tajima T and Dawson J M 1979 *Phys. Rev. Lett.* **43** 267
[41] Rosenzweig J B, Breizman B, Katsouleas T and Su J J 1991 *Phys. Rev. A* **44** R6189
[42] Li S, Li G Y, Ain Q, Hur M S, Ting A C, Kulagin V V, Kamperidis C and Hafz N A M 2019 *Sci. Adv.* **5** eaav7940

[43] Agostinelli S, Allison J, Amako K, *et al*. 2003 *Nucl. Instrum. Meth. A* **506** 250
[44] Allison J, Amako K, Apostolakis J, *et al*. 2006 *IEEE Trans. Nucl. Sci.* **53** 270
[45] Krasheninnikov A V and Nordlund K 2010 *J. Appl. Phys.* **107** 071301
[46] Stuchbery A E and Bezakova E 1999 *Phys. Rev. Lett.* **82** 3637
[47] Meldrum A, Zinkle S J, Boatner L A, *et al*. 1998 *Nature* **395** 56
[48] Rubia TDdl, Averback R S, Benedek R, *et al*. 1987 *Phys. Rev. Lett.* **59** 1930
[49] Trautmann C, Klaumünzer S and Trinkaus H 2000 *Phys. Rev. Lett.* **85** 3648
[50] Samela J and Nordlund K 2007 *Phys. Rev. B* **76** 125434
[51] Meyer J C, Eder F, Kurasch S, *et al*. 2012 *Phys. Rev. Lett.* **108** 196102
[52] Ferrari A C and Robertson J 2000 *Phys. Rev. B* **61** 14095